

Revisiting Mid-Level Patterns for Cross-Domain Few-Shot Recognition

Yixiong Zou
Peking University

Shanghang Zhang
University of California, Berkeley

JianPeng Yu
Carnegie Mellon University

Yonghong Tian*
Peking University

José M. F. Moura
Carnegie Mellon University

ABSTRACT

Existing few-shot learning (FSL) methods usually assume base classes and novel classes are from the same domain (in-domain setting). However, in practice, it may be infeasible to collect sufficient training samples for some special domains to construct base classes. To solve this problem, cross-domain FSL (CDFSL) is proposed very recently to transfer knowledge from general-domain base classes to special-domain novel classes. Existing CDFSL works mostly focus on transferring between near domains, while rarely consider transferring between distant domains, which is in practical need as any novel classes could appear in real-world applications, and is even more challenging. In this paper, we study a challenging subset of CDFSL where the novel classes are in distant domains from base classes, by revisiting the mid-level features, which are more transferable yet under-explored in main stream FSL work. To boost the discriminability of mid-level features, we propose a residual-prediction task to encourage mid-level features to learn discriminative information of each sample. Notably, such mechanism also benefits the in-domain FSL and CDFSL in near domains. Therefore, we provide two types of features for both cross- and in-domain FSL respectively, under the same training framework. Experiments under both settings on six public datasets, including two challenging medical datasets, validate the our rationale and demonstrate state-of-the-art performance. Code will be released.

CCS CONCEPTS

• Computing methodologies → Computer vision.

KEYWORDS

Cross-domain few-shot learning; Mid-level features

ACM Reference Format:

Yixiong Zou, Shanghang Zhang, JianPeng Yu, Yonghong Tian, and José M. F. Moura. 2021. Revisiting Mid-Level Patterns for Cross-Domain Few-Shot Recognition. In *Proceedings of the 29th ACM International Conference on*

*Corresponding author. Email: yhtian@pku.edu.cn

Permission to make digital or hard copies of all or part of this work for personal or classroom use is granted without fee provided that copies are not made or distributed for profit or commercial advantage and that copies bear this notice and the full citation on the first page. Copyrights for components of this work owned by others than ACM must be honored. Abstracting with credit is permitted. To copy otherwise, or republish, to post on servers or to redistribute to lists, requires prior specific permission and/or a fee. Request permissions from permissions@acm.org.

MM '21, October 20–24, 2021, Chengdu, China
© 2021 Association for Computing Machinery.
ACM ISBN 978-x-xxxx-xxxx-x/YY/MM...\$15.00
<https://doi.org/10.1145/nnnnnnn.nnnnnnn>

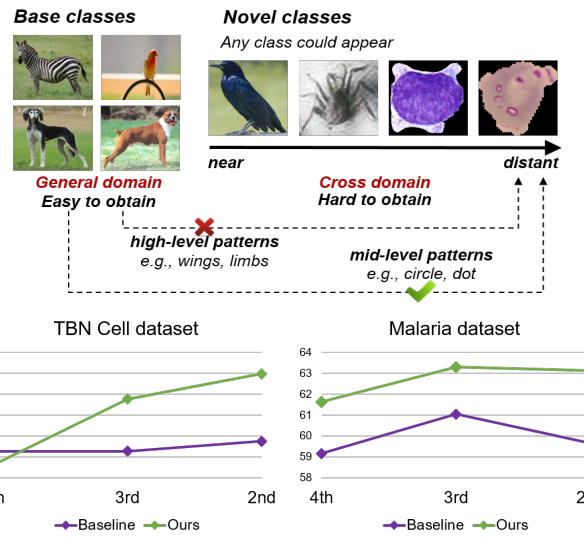


Figure 1: Top: In real-world applications of few-shot learning, any class could appear in novel classes, making it important to consider the situation where the novel classes are in the distant domains from base classes, which is rarely studied currently. To transfer knowledge from easy-to-obtain base classes in the general domain to novel classes in the distant domain (a challenging subset of cross-domain few-shot recognition), we revisit mid-level patterns that are more transferable than high-level patterns. Bottom: Quantitative evaluation of features from different blocks of ResNet when transferring base-class trained model to distant cross-domain datasets, where mid-level features (3rd and 2nd blocks) could show better performance compared with the high-level features (4th block, i.e., the last layer).

Multimedia (MM '21), October 20–24, 2021, Chengdu, China. ACM, New York, NY, USA, 9 pages. <https://doi.org/10.1145/nnnnnnn.nnnnnnn>

1 INTRODUCTION

Few-shot learning (FSL) [41] has been proposed recently to recognize objects in novel classes given only few training samples, with knowledge transferred from base classes (classes with sufficient training samples). Existing FSL works [31, 41] usually assume the in-domain setting, where base classes and novel classes are from the same domain. However, such setting may not stand in practice, because for domains where data is hard to obtain, it may be infeasible to collect sufficient training samples from them to construct

the base classes either. To solve this problem, very recently, cross-domain FSL (CDFSL) [5, 40] has been proposed to handle a more realistic setting where data from the general domain (which is easier to collect [5], e.g., ImageNet [8]) are sampled as base classes, while data from other domains are defined as novel classes. Compared with the general domain, the novel-class domains may contain semantic shift (general-domain to birds [5]), style-shift (natural images to pencil-paintings [48]), or both [14] (general-domain to medical microscopic images), as shown in Fig. 1. The novel-class domains may vary from being close to being distant against the base-class domain [14], because no assumptions should be made about what novel classes would appear in real-world applications.

However, existing CDFSL works [5, 40] mostly focus on the transferring between domains that are near from each other, while rarely consider that for distant domains. For instance, some specialized domains such as medical domains, which are very different from the general domain, could appear as novel classes in real-world applications, and transferring knowledge from general-domain could help the cold-start of the model training and benefit the downstream fine-tuning. Therefore, in this paper, we aim to solve a more challenging subset of the CDFSL problem where base classes and novel classes are from distant domains, termed as *distant-domain FSL* for abbreviation. Moreover, to facilitate the definition of distant domains, we also use the Proxy-A-Distance (PAD) [4, 10] to quantitatively measure domain distances (Tab. 1 and section 4.2).

To address distant-domain FSL, the model should learn transferable patterns from general-domain base classes and transfer them to distant-domain novel classes. Much work [46] on transfer learning suggests features from shallower (mid-level) layers are more transferable than those from deeper layers. Intuitively, as shown in Fig. 1 (top), high-level patterns from the general domain, such as wings and limbs, can hardly be transferred to distant-domain novel classes, while mid-level patterns, such as circle and dot, are easier to be transferred. Quantitatively, as shown in Fig. 1 (bottom), mid-level features from the third and second blocks of ResNet [16] could show better performance than the high-level features from the forth block (i.e., the last block) when transferring base-class trained model to distant-domain datasets¹. The utilization of mid-level features has been widely explored in the research on transfer learning [25], yet it is far from being well explored in FSL. Therefore, in this paper, we revisit mid-level features to learn transferable and discriminative mid-level features for distant-domain FSL.

Although mid-level features are more transferable than high-level features, they may not be discriminative enough. To boost their discriminability, during the base-class training, we design a residual-prediction task to encourage mid-level features to learn the discriminative information of each sample. The insight is that we assume each class has its unique character that could not be easily described by high-level patterns from other classes, while mid-level patterns can be more effective to describe it. Such unique character provides information to learn more discriminative mid-level features. Intuitively, for example in Fig. 1, to describe the unique character of zebra, zebra stripes, with knowledge from dogs, it is

¹To avoid ambiguity, we denote the feature/pattern of the last layer of the backbone network as high-level feature/pattern, and denote the feature/pattern of the layers other than the first and the last layer as the mid-level feature/pattern. For backbone with skip connections, the intermediate layers within skip connections are not used.

hard to use high-level patterns (e.g., high-level semantic part [37]) from dogs, while it is much easier to use mid-level patterns such as stripe to describe it, which indicates such unique character provides suitable information to facilitate the learning of more discriminative mid-level features. Moreover, as an example, such stripe-like pattern could help the medical analysis [32], i.e., distant-domain recognition. Specifically, we first extract features for base-class samples with the backbone network being trained by classifying such sample into N base classes. Then, for each training sample, we use high-level patterns from other $N - 1$ base classes to reconstruct the extracted feature, and obtain the residual feature by **removing** the reconstructed feature from the extracted feature. Such residual feature contains the discriminative information of this sample that is suitable for the mid-level features to learn. Finally, we choose all layers in the backbone network other than the first layer and the last layer to be the mid-layer set, layer-wisely learn weights for all the corresponding mid-level features, and force the weighted combined mid-level features to predict the discriminative residual features, which encourages mid-level features to be discriminative.

Note that although we aim at boosting the distant-domain FSL, our method is also effective for in-domain FSL and CDFSL in near domains. The base-class training process designed above is a pseudo-novel-class training strategy, which views the current training sample as a pseudo-novel-class sample, providing simulated in-domain novel-class data, and views the other classes as pseudo-base classes. As adequate information is provided when classifying such sample into base classes, its feature can be viewed as the ground truth for the pseudo-novel training process, and we are trying to predict such pseudo-novel features by reconstructing them via high-level patterns from pseudo-base classes. The lower bound of the reconstruction loss validates our assumption that each class has its unique character (Tab. 10). On the other hand, by predicting the discriminative pseudo-novel residual features, we are also encouraging the model to have the capability to predict real residual features for the real novel-class samples. Combining the predicted high-level feature and residual feature would output the whole predicted feature for the in-domain and near-domain novel class sample, thus boosting the in-domain FSL and CDFSL in near domains. Therefore, we provide two types of features for both distant-domain and in/near-domain novel-class recognition respectively, under the same training framework, according to the quantitative measure of domain distances by the Proxy-A-Distance (PAD) [10]. For distant-domain novel classes, we use the weighted concatenation of mid-level features in the candidate mid-layer set as the final feature. For in-domain or near-domain novel classes, we use all base-class prototypes to perform the high-level feature reconstruction, and combine it with the predicted residual term to be the final feature. Finally, the nearest neighbor classification will be performed for the novel-class recognition for all settings.

In all, our contributions can be summarized as follows:

- To solve CDFSL in distant domains, we revisit mid-level features to explore their transferability and discriminability, which is seldom studied in the main-stream FSL work.
- To enhance the discriminability of mid-level features, we propose a residual-prediction task to explore the unique character of each class.

- Our method is effective for not only the distant-domain FSL but also the in-domain FSL and near-domain CDFSL with different types of descriptive features. Experiments under both settings on six public datasets, including two challenging medical datasets, demonstrate state-of-the-art performance. Code will be released.

2 RELATED WORK

Few-shot learning methods can be roughly grouped into embedding based method [11, 41, 44], meta-learning based method [2, 9, 28], and hallucination based method [15, 43]. The pseudo-novel-class strategy is also adopted in [12]. Very recently, some works [5, 6, 39, 40, 48] studied the problem of cross-domain FSL, which train the model on general-domain classes and evaluate it on novel classes from other domains. [40] proposed to insert affine transformations sampled from the Gaussian distribution to intermediate layers to help the generalization. [48] proposed to utilize the domain adversarial adaptation mechanism to handle the style shift problem. We also study the problem of cross-domain FSL, and focus on a more challenging subset of it, i.e., distant-domain FSL.

Transferability of deep networks has been researched in the field of transfer learning [46], which shows an decreasing trend of transferability when going deeper into the deep network. Such phenomenon has also been applied in applications such as [25]. Some works [21, 23, 24] in FSL utilize features of multiple appended layers to handle the hierarchy of classes. The only work makes use of mid-level features, to the best of our knowledge, is [18], which directly applied mid-level features to the classification. In all, the usage of mid-level features is far from being well explored in FSL yet, which we revisit in this paper to boost both the distant-domain and the in/near-domain FSL.

3 METHODOLOGY

To learn transferable and discriminative mid-level features, we propose a residual-prediction task to explore the unique character of each class, which will benefit both the distant- and in/near-domain FSL. The framework is shown in Fig. 2.

3.1 Preliminaries

Few-shot learning (FSL) aims at recognizing novel classes given only few training samples. Following the setting of current works [34], we are provided with both base classes C^{base} with sufficient training samples, and novel classes C^{novel} where only few training samples are available. Note that C^{base} and C^{novel} are non-overlapping. The difference between in-domain FSL and cross-domain FSL lies in whether C^{base} and C^{novel} are from the same domain [5]. Few-shot learning is conducted on the training set (a.k.a. support set) of C^{novel} , and the evaluation is carried on the corresponding testing set (a.k.a. query set). For a fair comparison, current works always conduct a K -way n -shot evaluation, which means K novel classes $\{C_i^U\}_{i=1}^K$ will be sampled from C^{novel} with n novel-class training samples $\{x_{ij}^U\}_{j=1}^n$ in each class. For each sampled dataset (i.e., $K \cdot n$ training samples + testing samples, a.k.a. episode), the nearest neighbor classification will be performed, which is represented as

$$\hat{y}_q = \arg \max_{y_i} P(y_i | x_q^U) = \arg \max_i \frac{e^{s(F(x_q^U), p_i^U)}}{\sum_{k=1}^K e^{s(F(x_q^U), p_k^U)}} \quad (1)$$

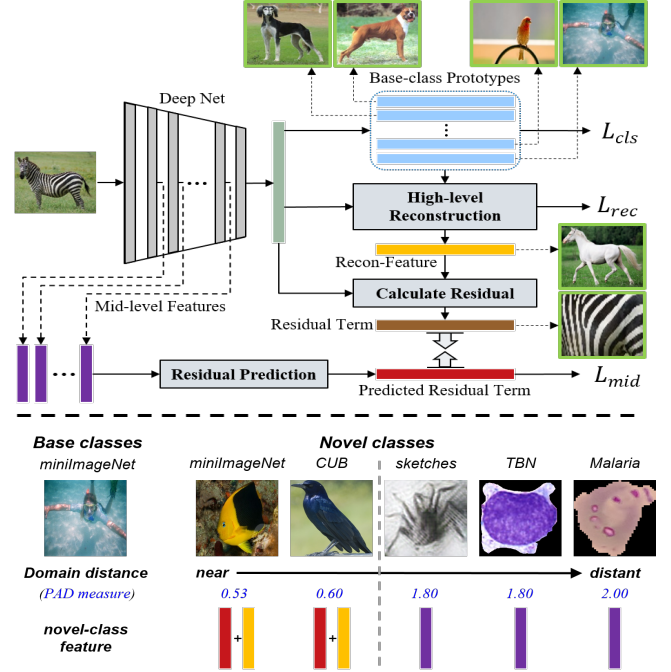


Figure 2: Framework. Top: Given an input (e.g., zebra) from base classes, besides classifying it into N base classes, we also conduct high-level feature reconstruction based on the other $N - 1$ base classes' prototypes (e.g., dogs, birds, human). Then the residual term will be calculated as the difference between the extracted feature and the reconstructed feature (e.g., zebra without stripes, maybe a white horse). Mid-level features from multiple mid-layers will be dynamically weighted to predict the residual term (e.g., stripes). Outlined images are the intuitive examples of connected terms. Such training will benefit both distant-domain and in/near-domain FSL. Bottom: When testing on novel classes, we provide two types of features for both distant-domain and in/near-domain novel classes respectively.

where $F()$ is the feature extractor, x_q^U is the testing sample (a.k.a. query sample), y_i refers to class C_i^U , \hat{y}_q is the estimated label for x_q^U , $s(\cdot)$ is the similarity function (e.g., cosine similarity), and p_i^U is the estimated prototype for class C_i^U , which is typically calculated as $p_i^U = \frac{1}{n} \sum_{j=1}^n F(x_{ij}^U)$ [36]. Based on \hat{y}_q , the performance will be evaluated on the sampled dataset. Repeat this sampling-evaluation procedure for hundreds of times, the performance of the evaluated model will be obtained.

Before the non-parametric training and testing on novel classes, the model also needs to be (pre-)trained on the base classes [34] to learn prior knowledges. In this work, we utilize the cosine classifier [5, 21] to be our baseline model, which is regarded as a simple but effective baseline. Given N base classes $\{C_i\}_{i=1}^N$, it trains the model by the cross-entropy loss given the input x and its label y as

$$L_{cls} = -\log(P(y|x)) = -\log\left(\frac{e^{\tau W_y^c f^c(x)}}{\sum_{i=1}^N e^{\tau W_i^c f^c(x)}}\right) \quad (2)$$

where $f(x) \in R^{d \times 1}$ is the extracted feature using the backbone $f()$, $W \in R^{N \times d}$ is the parameter for the fully connected (FC) layer, the superscript c denotes the vector is L_2 normalized ($W_i^c = W_i / \|W_i\|_2$, $f^c(x) = f(x) / \|f(x)\|_2$), and τ is a pre-defined hyper-parameter. We follow [31] to abandon the biases term of the FC layer. As the forward pass of the FC layer is equivalent to the calculation of the cosine similarity of W_i^c and $f^c(x)$, this baseline is named the cosine classifier. After the training on C^{base} , the backbone will be applied directly as the feature extractor for novel classes (i.e., set $F = f$ in Eq. 1), and the nearest neighbor classification will be performed.

3.2 Residual-prediction task

Although mid-level patterns could be more transferable than high-level ones [46], they may not be discriminative enough. Therefore, to boost the discriminability of mid-level features, we propose a residual-prediction task for the base-class training which encourages mid-level features to learn the discriminative information in each sample. Intuitively, for example, to describe zebra with knowledge from dogs, it is easy to transfer high-level patterns such as feet, tail to zebra. But for zebra's unique character, zebra stripes, it is hard to transfer high-level patterns (e.g., semantic parts [37]) from dogs, but it is much easier to transfer mid-level patterns such as stripe itself to describe it. Also, as an example, such stripe-like pattern could help the medical analysis [32], i.e., distant-domain recognition. Inspired by this, we assume every class has its unique character that could not be easily described by high-level patterns from other classes, for which mid-level patterns can be more effective, providing discriminative information suitable for mid-level features to learn. To improve mid-level features with such information, the residual prediction task can be divided into the following steps as shown in Fig. 2 (top): we first extract the feature for each base-class sample (e.g., zebra) with the backbone network being trained by the classification loss in Eq.2. Then, for each sample, we design to use high-level patterns from other classes (e.g., dogs, birds, human) to reconstruct the extracted feature (high-level reconstruction), and we **remove** the reconstructed feature (e.g., zebra without stripe, maybe a white horse) from the extracted feature, outputting a discriminative residual feature (e.g., stripes), which contains the discriminative information for this sample that is suitable for mid-level features to learn. Finally, we constrain mid-level features to predict such discriminative residual feature, which pushes mid-level features to be discriminative. Our method is jointly trained with L_{cls} and the residual-prediction task. Details are in the following.

3.2.1 High-level Reconstruction. Firstly, given a base-class training sample x , we use high-level patterns from other base classes to represent (reconstruct) its extracted feature $f(x)$. Current works [12, 31] suggest that the parameters of the base-class FC parameters W could be viewed as the prototypes of base classes, and each row of W (a prototype) contains the overall information of the corresponding class, which refers to the high-level patterns because it exists in the same feature space as that of the backbone's final layer. Therefore, prototypes are used to reconstruct $f(x)$. The prototypes of the other $N - 1$ base classes for x is denoted as the prototype set $\{W_i\}_{i \neq y}$ where y is the label of x and $W_i \in R^d$ is the same as the corresponding row in the FC parameters W .

The reconstruction is based on the feature and prototypes averagely split along the channel axis. For easy understanding, we

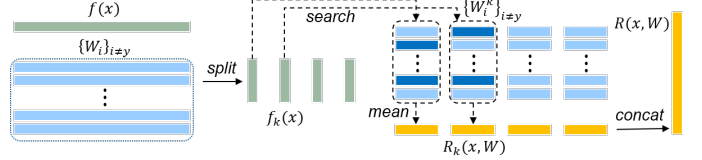


Figure 3: Illustration of high-level reconstruction.

begin with the situation where no splitting is applied. Specifically, we use the extracted feature $f(x)$ to apply the nearest neighbor search over $\{W_i\}_{i \neq y}$, and query top m prototypes with the highest cosine similarities to form the neighboring prototype set $\{\tilde{W}_i\}_{i=1}^m$. Then, the reconstructed feature is calculated as the mean of all queried prototypes as $R(x, W) = \frac{1}{m} \sum_{i=1}^m \tilde{W}_i$.

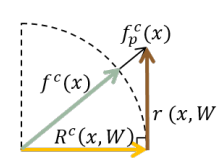
To provide a better reconstruction of the extracted feature, we split the extracted feature $f(x)$ averagely into S splits along the channel axis, denoted as $\{f_k(x)\}_{k=1}^S$ where $f_k(x) \in R^{d/S \times 1}$, i.e., concatenate all split features in $\{f_k(x)\}_{k=1}^S$ could obtain the original feature $f(x)$. We also split each prototype into S splits along the channel axis, where each split of prototypes is denoted as $\{W_i^k\}_{i \neq y}$, where $W_i^k \in R^{1 \times d/S}$. Then, the above nearest neighbor searching are conducted split-wisely between each $f_k(x)$ and $\{W_i^k\}_{i \neq y}$, outputting a split of reconstructed feature $R_k(x, W) \in R^{d/S \times 1}$, and finally the reconstructed feature $R(x, W) \in R^{d \times 1}$ is the concatenation of all splits of reconstructed features, as in Fig. 3. As the queried neighboring prototypes can be different across each split group k , the splitting operation can provide a closer reconstruction of $f(x)$ compared with directly applying the whole feature (Tab. 10).

Then, we constrain the reconstructed feature to be close to $f(x)$ in the cosine similarity space with the loss

$$L_{recon} = \|f^c(x) - R^c(x, W)\|_2^2 \quad (3)$$

where $R^c(x, W)$ is the L_2 normalized $R(x, W)$. Note that by applying this loss, we are also trying to decompose $f(x)$ into the split prototypes, which implicitly integrates the composition information of base classes into the feature, improving the in-domain FSL.

3.2.2 Residual Calculation. In experiments (Tab. 10), we find that for the best case that $f(x)$ could be improved for in-domain FSL, L_{recon} remains about 0.11 to 0.25. Keeping enlarging the weight of L_{recon} will largely decrease the performance, indicating the best case that the high-level reconstruction can reach, which verifies our assumption that every class has its character that could not be easily represented by high-level patterns from other classes. By removing the high-level patterns from $f(x)$, we will get a discriminative residual feature which contains the discriminative information suitable for mid-level features to learn.



As both $f^c(x)$ and $R^c(x, W)$ are L_2 normalized, these vectors can be viewed to be distributed on a unit circle (left figure). Intuitively, the residual term and the high-level reconstructed term should not be representative of each other, which implies they should be orthogonal. Therefore, we prolong the L_2 normalized feature $f^c(x)$ to $f_p^c(x)$ by $f_p^c(x) =$

$f^c(x)/\cos\langle f^c(x), R^c(x, W) \rangle$, where the cosine value could be obtained as $1 - L_{recon}/2$. Moreover, this prolonging could also stabilize the training. Thus, the residual is calculated as $r(x, W) = f_p^c(x) - R^c(x, W) \in R^{d \times 1}$.

3.2.3 Residual Prediction. Then, to boost the discriminability of the mid-level features, we utilize the mid-level feature to predict the residual term. The predicted residual term is the weighted combination of multiple transformed mid-level features from a fixed mid-layer set $\{m_l(x)\}_{l=1}^L$ where L is the number of total candidate mid-layers and $m_l(x) \in R^{d_l \times 1}$ is the mid-level feature for layer l . For better understanding, we begin with the scenario where only one mid-layer $m_l(x)$ is used in residual prediction, and the weighted combination of multiple layers will be included afterwards.

As a vector can be decomposed into its direction (L_2 normalized vector) and length (L_2 norm), we can re-write the residual term as

$$r(x, W) = \frac{r(x, W)}{\|r(x, W)\|_2} \cdot \|r(x, W)\|_2 = r^c(x, W) \cdot \|r(x, W)\|_2 \quad (4)$$

In practice, we find it is beneficial to predict the direction ($r^c(x, W)$) and the length $\|r(x, W)\|_2$ of the residual term separately. For better understanding, we first introduce the prediction of the residual term's direction, which is similar to the prediction of its length. Therefore, firstly our aim is to transform a mid-level feature $m_l(x)$ to predict $r^c(x, W)$. As it is the mid-level feature instead of another high-level feature that is what we want, we should avoid learning another high-level feature by utilizing any deep and complex transformation network during the prediction. Therefore, we simply transform the mid-level feature by multiplying a matrix and adding a bias on it, which is calculated as

$$\hat{r}_l^c(x, W) = \frac{W_l^r m_l(x) + b_l^r}{\|W_l^r m_l(x) + b_l^r\|_2} \quad (5)$$

where $W_l^r \in R^{d \times d_l}$ and $b_l^r \in R^{d \times 1}$ are the weights and the biases for the transformation, and d_l is the dimension of layer l . The prediction is also L_2 normalized to represent a direction, which simplifies the prediction.

Similarly, the prediction of the residual term's length $\|r(x, W)\|_2$ (a scalar) is also performed by a simple transformation as

$$\hat{r}_l^s(x, W) = W_l^s m_l(x) + b_l^s \quad (6)$$

where $W_l^s \in R^{d_l}$ and $b_l^s \in R$ are the corresponding parameters.

Given the predicted direction and length from $m_l(x)$, the predicted residual term can be represented as $\hat{r}_l(x, W) = \hat{r}_l^c(x, W) \cdot \hat{r}_l^s(x, W) \in R^{d \times 1}$, and we design a loss as $\|\hat{r}_l^c(x, W) - r^c(x, W)\|_2^2 + \alpha(\hat{r}_l^s(x, W) - \|r(x, W)\|_2)^2$ to separately push the direction and length to be close to the residual term.

For the prediction from multiple mid-layers, we learn two weights for each layer's predicted direction and predicted length respectively, which are denoted as $a_l(x)$ and $a_l^s(x)$ and calculated as

$$a_l(x) = \frac{t_l(m_l(x))}{\sum_{k=1}^L t_k(m_l(x))}; \quad a_l^s(x) = \frac{t_l^s(m_l(x))}{\sum_{k=1}^L t_k^s(m_l(x))} \quad (7)$$

where $t_l()$ and $t_l^s(x)$ are implemented as two independent single-layer perceptrons appended to the corresponding mid-level feature $m_l(x)$ and each will output a scalar value. With these layer-wise

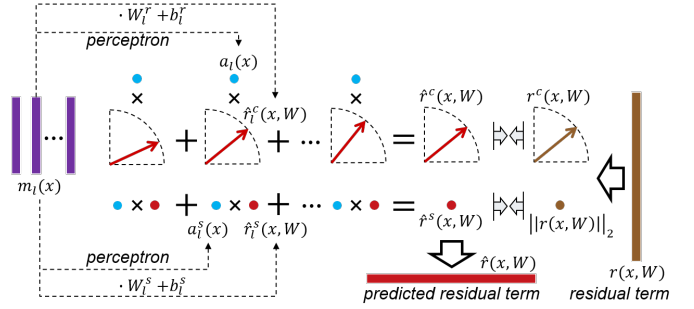


Figure 4: Illustration of residual prediction. Each circle denotes a scalar, each arrow in a sector denotes a L_2 normalized vector, and blue circles denote the layer weights. Since a vector can be decomposed into its direction (L_2 normalized vector) and length (L_2 norm), we separately predict the residual term's direction $r^c(x, W)$ (brown arrow) and length $\|r(x, W)\|_2$ (brown circle). The predicted direction $\hat{r}^c(x, W)$ and length $\hat{r}^s(x, W)$ are the weighted combination of the each direction $\hat{r}_l(x, W)$ and $\hat{r}_l^s(x, W)$ which are transformed from each mid-layer $m_l(x)$, and are weighted by the layer specific weights $a_l(x)$ and $a_l^s(x)$ (blue circles).

weights, we can simply use a fixed candidate mid-layer set to include all layers other than the first and the last layer.

Then, the weighted combination of the predicted direction and length from multiple mid-layers can be represented as

$$\begin{aligned} \hat{r}^c(x, W) &= \frac{\sum_{l=1}^L a_l(x) \cdot \hat{r}_l^c(x, W)}{\|\sum_{l=1}^L a_l(x) \cdot \hat{r}_l^c(x, W)\|_2} \\ \hat{r}^s(x, W) &= \sum_{l=1}^L a_l(x) \cdot \hat{r}_l^s(x, W) \end{aligned} \quad (8)$$

Finally, the prediction loss which separately pushes the direction and length to be close is calculated as

$$L_{mid} = \|\hat{r}^c(x, W) - r^c(x, W)\|_2^2 + \alpha(\hat{r}^s(x, W) - \|r(x, W)\|_2)^2 \quad (9)$$

where $r^c(x, W)$ and $\|r(x, W)\|_2$ is the direction and length of the residual term respectively, and α is a pre-defined hyper-parameter. The first part of L_{mid} is the direction prediction loss, and the second part is the length prediction loss. This process is shown in Fig. 4.

The final loss for base-class training is

$$L = L_{cls} + \lambda_1 L_{recon} + \lambda_2 L_{mid} \quad (10)$$

where λ_1 and λ_2 are predefined hyper-parameters.

3.3 Novel-class Recognition

Although we aim to boost mid-level features for distant-domain classes, this framework is also effective for in-domain FSL and CDFSL in near domains. We provide two novel-class features under the same training framework, for both the distant- and in/near-domain settings respectively as shown in Fig. 2 (bottom), according to the quantitative domain distance measure by PAD [10].

3.3.1 Distant-domain. As all mid-level features within the candidate mid-feature set are improved but they are of different feature dimensions, we use the weighted concatenation of all mid-level features as the final feature as

Table 1: Datasets and quantitative domain distances.

Dataset	Classes	Samples	Train/val/test class number	PAD
miniImageNet	100	60,000	64 / 16 / 20	0.53
CUB-200-2011	200	11,788	100 / 50 / 50	0.60
Kinetics	100	6,400	64 / 12 / 24	-
Pencil-paintings*	36	21,600	- / 16 / 20	1.80
TBN cell*	3	363	- / - / 3	1.80
Malaria cell*	2	27,558	- / - / 2	2.00

$$F(x) = \text{concatenate}(\{a_l(x) \cdot m_l^c(x)\}_{l=1}^L) \quad (11)$$

where $F(x)$ is the final feature in Eq. 1, and $\{m_l^c(x)\}_{l=1}^L$ is the L_2 normalized candidate mid-feature set with the weight $a_l(x)$ in Eq. 7 for each layer. For clarity we denote this distant-domain feature as $F_a(x)$. The ablation study of each mid-feature is validated in Tab. 8. 3.3.2 *In/near-domain*. The base-class training stated above is actually a pseudo-novel training strategy, which views the current sample x as a pseudo-novel-class sample and views other classes as pseudo-base classes for it, providing simulated in-domain novel-class data. As adequate information is provided for L_{cls} , the extracted pseudo-novel feature $f(x)$ can be viewed as the ground truth for such pseudo-novel training. By encouraging the high-level reconstruction from pseudo-base classes, we are trying to predict the pseudo-novel feature $f(x)$ merely based on pseudo-base prototypes $\{W_i\}_{i \neq y}$. By predicting the discriminative pseudo-novel residual feature, we are also encouraging the model to predict the real discriminative residual feature for the (real) novel-class feature. After such training, on base classes the model will be able to predict the discriminative pseudo-novel feature $f(x)$, merely based on the pseudo-base-class prototypes $\{W_i\}_{i \neq y}$ and mid-level features, which makes it able to predict the discriminative in/near-domain (real) novel-class feature, thus helping the in/near-domain FSL.

Therefore, we use all base-class prototypes to conduct the high-level reconstruction, and then the reconstructed feature together with the predicted residual term will be combined to be the final feature, which is calculated as

$$F(x) = R^c(x, W) + \hat{r}^s(x, W) \cdot \hat{r}^c(x, W) \quad (12)$$

For clarity we denote this in/near-domain feature as $F_b(x)$.

Finally, the nearest neighbor classification based on Eq. 1 will be conducted and obtain the final performance.

4 EXPERIMENTS

Extensive experiments are conducted under both distant-domain and in/near-domain FSL settings. Due to space limitation, more details are included in the supplementary material.

4.1 Datasets and Settings

Datasets used for evaluation are summarized in Tab. 1, where *val* denotes validation, and * denotes distant-domain datasets, including Pencil-paintings dataset [48] and two medical datasets² (TBN Cell [30] and Malaria Cell [33]). miniImageNet [41] is a subset of ImageNet [8] and the pencil-paintings dataset contains novel classes of miniImageNet converted to the pencil-painting images. The CUB [42] dataset is a fine-grained dataset of birds, and the

²TBN Cell [30]: <http://mcs.sat.psu.ac.th/dataset/dataset.zip> Malaria Cell [33]: <https://lhn-cbc.cdc.nlm.nih.gov/publication/pub9932>

Kinetics dataset [51] contains video actions. Some examples can be found in Fig. 2 (bottom). For the distant-domain setting, the listed datasets are used as novel classes, and the base classes of miniImageNet are used as base classes [5]. Following existing methods [41], the mean accuracy (%) and the 95% confidence intervals of randomly generated K -way n -shot episodes from test sets (novel classes) will be reported.

4.2 Quantitative Measure of Domain Distances

We first utilize Proxy-A-Distance (PAD) [4, 10] for quantitative domain distance measuring. As miniImageNet is used as the base classes for all the distant-domain evaluation, we calculate the PAD between all candidate domains' novel classes with base classes from miniImageNet. Details are in supplementary materials, results are listed in the last column of Tab. 1.

As miniImageNet's base and novel classes are from the same domain [41], the distance between these two set could be viewed as the lower bound for the PAD. From Tab. 1 we can see that the PAD of CUB is quite close to this lower bound, indicating this dataset should be used as the CDFSL dataset that is in the near domain of miniImageNet. The pencil-paintings is the third distant domain. Unsurprisingly that it is closer than two medical datasets as it shares semantically similar classes with base classes of miniImageNet, but is **much more distant** than CUB. Therefore, we use this dataset as a distant domain. The two medical datasets are the furthest datasets, with the Malaria cell dataset reaches the upper bound of PAD (2.0), so these two datasets are also selected as distant domains.

4.3 Implementation Details

Due to the space limitation, detailed parameter settings are in the supplementary material. For the CUB benchmark, we follow current works [31, 38, 45] to use the provided bounding boxes to crop the images. For the Kinetics dataset, to handle the temporal information, we uniformly sample 8 frames from the video, and a temporal convolution layer with the kernel of $8 \times 1 \times 1$ is appended to the backbone network. For all the above models, the mid-level feature maps of size $h_l \times w_l \times d_l$ ($t_l \times h_l \times w_l \times d_l$) is global averaged in all dimensions except the last one to obtain the mid-level feature. As all elements in extracted features are positive due to the ReLU [13] activation, to constrain prototypes in the same feature space as the extracted features, we also apply an *abs()* function to FC parameters to use the absolute values. For medical datasets, to preserve resolutions, we use raw images from ImageNet as base classes [14].

4.4 Comparison with State-of-the-art

4.4.1 *Distant-domain Setting*. We report our performance under the distant-domain FSL setting in Tab. 2 and Tab. 3, together with state-of-the-art works implemented by us. We denote the weighted concatenation of mid-features (i.e., $F_a()$) as *Ours_a* in both tables. All models are trained on base classes of miniImageNet. We use ResNet12 [16] as the backbone network and use features of the third block and second block to form the mid-layer candidate set. From these tables we can see that our method outperforms the state-of-the-art methods on all three datasets.

4.4.2 *In/near-domain Setting*. To compare our method with current works in the in/near-domain setting, we report the performance of ours and that of others in Tab. 5, 6 and 7 under the in-domain setting, and report the comparison of CDFSL in near domains in Tab. 4.

Table 2: Distant-domain performance on pencil-paintings.

Method	5-way 1-shot	5-way 5-shot
MatchingNet [41]	23.35 ± 0.64	32.42 ± 0.55
RelationNet [44]	23.87 ± 0.82	33.29 ± 0.96
PPA [31]	23.86 ± 0.42	33.74 ± 0.41
SGM [43]	23.49 ± 0.29	32.67 ± 0.32
ProtoNet [36]	23.23 ± 0.32	32.92 ± 0.41
MetaOptNet [20]	24.53 ± 0.20	33.23 ± 0.63
Baseline++ [5]	24.06 ± 0.46	32.74 ± 0.81
LFT+GNN [40]	27.02 ± 0.43	34.28 ± 0.43
DAPN [48]	27.25 ± 0.25	37.45 ± 0.25
Cosine Classifier	28.19 ± 0.24	37.21 ± 0.37
Ours _a	29.45 ± 0.22	40.38 ± 0.35

Table 3: Distant-domain performance on medical datasets.

Method	TBN cell (3-way)		Malaria cell (2-way)	
	1-shot	5-shot	1-shot	5-shot
Pixel	44.03 ± 0.27	51.95 ± 0.38	53.01 ± 0.40	53.79 ± 0.53
Random Init	48.38 ± 0.33	55.87 ± 0.44	52.75 ± 0.36	55.78 ± 0.58
MatchingNet [41]	44.40 ± 0.31	60.52 ± 0.43	53.92 ± 0.38	57.65 ± 0.54
DAPN [48]	54.18 ± 0.38	64.56 ± 0.29	55.22 ± 0.40	63.88 ± 0.37
ProtoNet [36]	59.56 ± 0.28	66.48 ± 0.39	58.12 ± 0.37	67.68 ± 0.55
Baseline++ [5]	56.89 ± 0.32	66.25 ± 0.40	60.47 ± 0.37	71.35 ± 0.48
MatchingNet+ [6]	51.54 ± 0.31	62.57 ± 0.39	59.97 ± 0.39	64.47 ± 0.52
ProtoNet+ [6]	60.07 ± 0.28	66.56 ± 0.38	59.85 ± 0.38	70.06 ± 0.52
LFT+GNN [40]	54.20 ± 0.39	67.13 ± 0.31	62.54 ± 0.52	74.51 ± 0.38
Multi-level [18]	61.71 ± 0.28	68.95 ± 0.40	60.86 ± 0.39	72.60 ± 0.54
Cosine Classifier	60.65 ± 0.28	68.96 ± 0.36	59.16 ± 0.35	70.41 ± 0.39
Ours _a	64.12 ± 0.26	72.88 ± 0.36	63.82 ± 0.41	76.94 ± 0.32

Table 4: Cross-domain performance on near domains (CUB).

Method	5-way 1-shot	5-way 5-shot
MatchingNet [41]	35.89 ± 0.51	51.37 ± 0.77
RelationNet [44]	42.44 ± 0.77	57.77 ± 0.69
ProtoNet [36]	–	62.02 ± 0.70
Baseline++ [5]	–	65.57 ± 0.70
DAPN [48]	47.47 ± 0.75	66.98 ± 0.68
Neg-Cosine [22]	–	67.03 ± 0.76
Cosine Classifier	45.97 ± 0.29	65.92 ± 0.24
Ours _b	48.81 ± 0.30	67.04 ± 0.61

The feature provided for the in/near-domain setting (i.e., $F_b()$) is denoted as $Ours_b$. For the *miniImageNet*, we include experiments of the *trainval* settings [20, 31, 35], where the validation set is included during training. In Tab.7, results of current works are directly obtained from [51] (without std). As shown in these tables, we outperform current works on CUB and Kinetics, and achieve comparable performance on *miniImageNet*.

4.5 Ablation Study

For better understanding, we report the ablation studies first for the in-domain FSL and then for the distant-domain FSL.

4.5.1 In-domain Setting. The performance of models implemented with different modules is in Tab. 9. Each row in the second column represents the model with modules of all the above rows plus the module in the current row. For the cosine classifier, $+abs$, and $+L_{recon}$, we use the backbone extracted feature as the final feature (i.e., $F = f$ in Eq. 1). For $+L_{mid}$, we use $F_b()$ as the final feature.

Table 5: In-domain image FSL on CUB (ResNet10).

Method	5-way 1-shot	5-way 5-shot
MatchingNet [41]	61.16 ± 0.89	72.86 ± 0.70
ProtoNet [36]	51.31 ± 0.91	70.77 ± 0.69
MAML [9]	55.92 ± 0.95	72.09 ± 0.76
RelationNet [44]	62.45 ± 0.98	76.11 ± 0.69
DEML+MetaSGD [50]	66.95 ± 1.06	77.1 ± 0.78
ResNet18+TriNet [7]	69.61 ± 0.46	84.10 ± 0.35
MAML++ [3]	67.48 ± 1.44	83.80 ± 0.35
SCA+MAML++ [3]	70.33 ± 0.78	85.47 ± 0.40
S2M2 [26]	72.40 ± 0.34	86.22 ± 0.53
CFA [17]	73.90 ± 0.80	86.80 ± 0.50
AssoAlign [1]	74.22 ± 1.09	88.65 ± 0.55
DeepEmb [47]	75.65 ± 0.83	88.69 ± 0.50
Cosine Classifier	71.37 ± 0.25	86.57 ± 0.46
Ours _b	77.65 ± 0.26	88.83 ± 0.48

Table 6: In-domain image FSL on *miniImageNet*.

Method	5-way 1-shot	5-way 5-shot
MatchingNet [41]	46.56 ± 0.84	55.31 ± 0.73
ProtoNet [36]	49.42 ± 0.78	68.20 ± 0.66
MAML [9]	48.70 ± 1.84	63.11 ± 0.92
RelationNet [44]	50.44 ± 0.82	65.32 ± 0.70
Dynamic FS [12]	55.45 ± 0.89	70.13 ± 0.68
SNAIL [27]	55.71 ± 0.99	68.88 ± 0.92
TADAM [29]	58.50 ± 0.30	76.70 ± 0.30
PPA (<i>trainval</i>) [31]	59.60 ± 0.41	73.74 ± 0.19
LEO (<i>trainval</i>) [35]	61.76 ± 0.08	77.59 ± 0.12
DCO [20]	62.62 ± 0.61	78.63 ± 0.46
DCO (<i>trainval</i>) [20]	64.09 ± 0.62	80.00 ± 0.45
MetaOptNet [20]	62.64 ± 0.61	78.63 ± 0.46
MetaOptNet (<i>trainval</i>) [20]	64.09 ± 0.62	80.00 ± 0.45
Cosine Classifier (ResNet10)	55.97 ± 0.26	74.95 ± 0.24
Ours _b (ResNet10)	62.01 ± 0.27	77.49 ± 0.63
Ours _b (<i>trainval</i> , ResNet10)	63.38 ± 0.69	78.72 ± 0.65
Cosine Classifier (ResNet12)	56.26 ± 0.28	74.97 ± 0.24
Ours _b (ResNet12)	63.06 ± 0.76	77.82 ± 0.58
Ours _b (<i>trainval</i> , ResNet12)	64.19 ± 0.78	80.01 ± 0.76

Table 7: In-domain video FSL on Kinetics (ResNet12).

Method	5-way 1-shot	5-way 5-shot
RGB w/o mem	28.7	48.6
Flow w/o mem	24.4	33.1
LSTM(RGB) w/o mem	28.9	49.0
Nearest-finetune	48.2	62.6
Nearest-pretrain	51.1	68.9
Matching Network [41]	53.3	74.6
MAML [9]	54.2	75.3
Plain CMN [19]	57.3	76.0
LSTM-cmb	57.6	76.2
CMN [51]	60.5	78.9
Cosine classifier	62.13 ± 0.27	77.81 ± 0.63
Ours _b	64.63 ± 0.64	79.10 ± 0.77

From this table we can see that each module contributes to the performance respectively. abs contributes because all the prototypes are constrained to be positive, which is the same as the extracted features, simplifying the training. L_{recon} also improves the performance because by encouraging the pseudo-novel feature close to the reconstructed feature, the network is pushed to learn the composition of base-class prototypes. Moreover, we can see that L_{recon} contributes the most to CUB by around 4%, exceeding that to all other datasets. On the other hand, for L_{mid} , on CUB this

Table 8: Ablation study by distant-domain 1-shot testing.

Case	Method	Forth Block (Final-layer)	Third Block (Mid-layer)	Second Block (Mid-layer)	Concatenation of mid-features (Ours _a)
Pencil ResNet12 5-way 1-shot	Cosine	28.19 ± 0.24	28.35 ± 0.23	27.21 ± 0.21	27.95 ± 0.23
	+abs	28.22 ± 0.21	28.84 ± 0.21	27.95 ± 0.22	28.89 ± 0.22
	+ L_{recon}	28.29 ± 0.22	28.12 ± 0.24	27.61 ± 0.24	28.12 ± 0.23
	+ L_{mid}	28.09 ± 0.21	29.21 ± 0.25	28.13 ± 0.22	29.45 ± 0.22
TBN Cell ResNet12 3-way 1-shot	Cosine	60.25 ± 0.28	60.27 ± 0.29	60.74 ± 0.27	60.55 ± 0.28
	+abs	62.22 ± 0.32	62.82 ± 0.29	62.05 ± 0.31	61.78 ± 0.28
	+ L_{recon}	58.66 ± 0.31	61.09 ± 0.30	60.57 ± 0.29	60.95 ± 0.27
	+ L_{mid}	59.61 ± 0.29	62.76 ± 0.27	63.98 ± 0.27	64.12 ± 0.26
Malaria Cell ResNet12 2-way 1-shot	Cosine	59.16 ± 0.35	61.04 ± 0.37	59.66 ± 0.38	59.90 ± 0.37
	+abs	59.50 ± 0.32	60.40 ± 0.36	58.86 ± 0.39	59.68 ± 0.38
	+ L_{recon}	58.83 ± 0.34	61.40 ± 0.39	59.97 ± 0.39	60.79 ± 0.38
	+ L_{mid}	61.63 ± 0.36	63.29 ± 0.35	63.14 ± 0.41	63.82 ± 0.41

Table 9: Ablation study under the in-domain setting.

Study Case	Method	5-way 1-shot (%)	5-way 5-shot (%)
CUB ResNet10	cosine classifier	71.37 ± 0.25	86.57 ± 0.46
	+ abs	72.84 ± 0.26	86.99 ± 0.23
	+ L_{recon}	76.47 ± 0.27	87.22 ± 0.24
	+ L_{mid}	77.65 ± 0.26	88.23 ± 0.48
minImageNet ResNet10	cosine classifier	55.97 ± 0.26	74.95 ± 0.24
	+ abs	57.83 ± 0.26	75.25 ± 0.71
	+ L_{recon}	59.15 ± 0.25	75.73 ± 0.83
	+ L_{mid}	62.01 ± 0.27	77.49 ± 0.63
Kinetics ResNet12	cosine classifier	62.13 ± 0.27	77.81 ± 0.63
	+ abs	62.67 ± 0.26	78.27 ± 0.61
	+ L_{recon}	63.59 ± 0.25	78.91 ± 0.60
	+ L_{mid}	64.63 ± 0.64	79.10 ± 0.77

term contribute less than that on *minImageNet*. This is because CUB is a fine-grained dataset for birds. As nearly all birds contain similar high-level patterns (e.g., wings, beak), the high-level feature reconstruction on CUB will be much easier than that on *minImageNet*. In *minImageNet*, various classes exist, such as dogs, cars, ships, which means these classes may not contain as many over-lapped high-level patterns as that on CUB, making the high-level feature reconstruction harder. Therefore, L_{recon} promotes more on CUB. Moreover, it can also explain why L_{mid} promotes more on *minImageNet* than CUB: As there are larger residual terms on *minImageNet* that could not be well reconstructed by prototypes, the mid-level prediction helps more.

4.5.2 Distant-domain Setting. The ablation study is in Tab. 8, with the feature of the forth (i.e., final), the third, the second block and the concatenation of the third and second block (i.e., $F_a()$). We can see that almost all forth blocks' features are outperformed by that of the third blocks, which is consistent with the study [46] that mid-level features can be more transferable than final-layer's feature, and verifies the choice of distant domain datasets. For this challenging setting, methods that helps the in-domain FSL cannot show significant improvements now, because by fitting the base classes (especially $+L_{recon}$), the model is likely to learn more about the domain-specific information which may harm the transferability. Meanwhile, by applying L_{mid} , we can see a clear improvement of mid-level features over baselines and the forth layer features, which verifies our motivation: boosting the discriminability of mid-level features by the residual-prediction task.

4.5.3 Comparison of high-level reconstruction. We trained our model with L_{recon} on *minImageNet* with different splits in Tab. 10, with

Table 10: Hyper-parameters of high-level feature reconstruction. Experiments are conducted on *minImageNet*.

Method	Segments	5-way 1-shot (%)	L_{recon}
Average over queried	without L_{recon}	-	57.83 ± 0.26
	1	58.25 ± 0.28	0.19
	4	59.15 ± 0.25	0.16
	16	58.94 ± 0.26	0.14
	64	58.21 ± 0.26	0.11

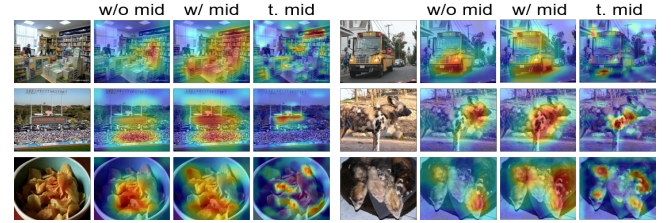


Figure 5: Visualization of the final-layer feature maps when trained with (w/) and without (w/o) L_{mid} , and the transformed mid-layer feature maps (t. mid). w/ mid cover more activated regions than w/o mid, where the difference can coarsely correspond to that of t. mid.

the optimal performance and the L_{recon} value. We can see by splitting the extracted feature and prototypes, the reconstructed feature gets closer to the extracted feature (L_{recon} decreases as splits increase), leading to the best feature implicitly encoded with base-class prototypes (setting splits to 4, obtaining the accuracy at 59.15). Also, we can see that for the best improved feature, L_{recon} remains larger than 0.1, which coarsely corresponds to an angle of 20° in the degree measure, verifying the existence of residual terms.

4.6 Visualization

To verify the contribution of mid-level patterns, we visualize the activated regions on novel classes of *minImageNet* in Fig. 5. As the high-level and mid-level representations are already implicitly encoded in the extracted feature, we visualize the final-layer feature maps of models trained with (w/) and without (w/o) the L_{mid} , together with the transformed mid-layer feature maps (t. mid), by means of summing up and resizing all the feature maps [49]. We can see the model trained without L_{mid} covers less activated regions than that trained with L_{mid} , indicating regions that are unable to be described by the baseline method are now better described by our model. The difference in the covered activated regions coarsely

corresponds to the activated regions of the transformed mid-layer feature maps, which verifies the contribution of mid-level patterns.

5 CONCLUSION

To learn transferable and discriminative mid-level features for the distant-domain FSL, we proposed a residual-prediction task consisting of the high-level feature reconstruction and the mid-level residual prediction, which consistently achieves state-of-the-art performance and better. Extensive experiments on both the distant- and in-domain settings including image recognition and video recognition show the rationale and the insights of the proposed method.

REFERENCES

- [1] Arman Afrasiyabi, Jean-François Lalonde, and Christian Gagné. 2020. Associative alignment for few-shot image classification. In *European Conference on Computer Vision*. Springer, 18–35.
- [2] Marcin Andrychowicz, Misha Denil, Sergio Gomez, Matthew W Hoffman, David Pfau, Tom Schaul, Brenden Shillingford, and Nando De Freitas. 2016. Learning to learn by gradient descent by gradient descent. In *NeurIPS*. 3981–3989.
- [3] Antreas Antoniou et al. 2019. Learning to learn by Self-Critique. *arXiv preprint arXiv:1905.10295* (2019).
- [4] Shai Ben-David, John Blitzer, Koby Crammer, and Fernando Pereira. 2007. Analysis of representations for domain adaptation. In *Advances in neural information processing systems*. 137–144.
- [5] Wei-Yu Chen, Yen-Cheng Liu, Zsolt Kira, Yu-Chiang Frank Wang, and Jia-Bin Huang. 2019. A Closer Look at Few-shot Classification. *CoRR* abs/1904.04232 (2019). arXiv:1904.04232 <http://arxiv.org/abs/1904.04232>
- [6] Yinbo Chen, Xiaolong Wang, Zhuang Liu, Huijuan Xu, and Trevor Darrell. 2020. A New Meta-Baseline for Few-Shot Learning. *arXiv preprint arXiv:2003.04390* (2020).
- [7] Zitian Chen, Yanwei Fu, Yinda Zhang, Yu-Gang Jiang, Xiangyang Xue, and Leonid Sigal. 2018. Semantic feature augmentation in few-shot learning. *arXiv preprint arXiv:1804.05298* 86 (2018), 89.
- [8] Jia Deng, Wei Dong, Richard Socher, Li-Jia Li, Kai Li, and Li Fei-Fei. 2009. Imagenet: A scale hierarchical image database. In *CVPR*. Ieee, 248–255.
- [9] Chelsea Finn, Pieter Abbeel, and Sergey Levine. 2017. Model-agnostic meta-learning for fast adaptation of deep networks. *arXiv preprint arXiv:1703.03400* (2017).
- [10] Yaroslav Ganin, Evgeniya Ustinova, Hana Ajakan, Pascal Germain, Hugo Larochelle, François Laviolette, Mario Marchand, and Victor Lempitsky. 2016. Domain-adversarial training of neural networks. *The Journal of Machine Learning Research* 17, 1 (2016), 2096–2030.
- [11] Victor Garcia and Joan Bruna. 2017. Few-shot learning with graph neural networks. *arXiv preprint arXiv:1711.04043* (2017).
- [12] Spyros Gidaris and Nikos Komodakis. 2018. Dynamic Few-Shot Visual Learning without Forgetting. In *CVPR*. 4367–4375.
- [13] Xavier Glorot, Antoine Bordes, and Yoshua Bengio. 2011. Deep sparse rectifier neural networks. In *AISTATS*. 315–323.
- [14] Yunhui Guo, Noel C Codella, Leonid Karlinsky, James V Codella, John R Smith, Kate Saenko, Tajana Rosing, and Rogerio Feris. 2019. A Broader Study of Cross-Domain Few-Shot Learning. (2019).
- [15] Bharath Hariharan and Ross Girshick. 2017. Low-shot visual recognition by shrinking and hallucinating features. In *ICCV*. 3018–3027.
- [16] Kaiming He, Xiangyu Zhang, Shaoqing Ren, and Jian Sun. 2016. Deep residual learning for image recognition. In *CVPR*. 770–778.
- [17] Ping Hu, Ximeng Sun, Kate Saenko, and Stan Sclaroff. 2019. Weakly-supervised Compositional Feature Aggregation for Few-shot Recognition. *arXiv preprint arXiv:1906.04833* (2019).
- [18] Shaoli Huang and Dacheng Tao. 2019. All you need is a good representation: A multi-level and classifier-centric representation for few-shot learning. *arXiv preprint arXiv:1911.12476* (2019).
- [19] Łukasz Kaiser, Ofir Nachum, Aurko Roy, and Samy Bengio. 2017. Learning to remember rare events. *arXiv preprint arXiv:1703.03129* (2017).
- [20] Kwonjoon Lee, Subhransu Maji, Avinash Ravichandran, and Stefano Soatto. 2019. Meta-learning with differentiable convex optimization. In *CVPR*. 10657–10665.
- [21] Aoxue Li, Tiange Luo, Zhiwu Lu, Tao Xiang, and Liwei Wang. 2019. Large-Scale Few-Shot Learning: Knowledge Transfer With Class Hierarchy. In *CVPR*. 7212–7220.
- [22] Bin Liu, Yue Cao, Yutong Lin, Qi Li, Zheng Zhang, Mingsheng Long, and Han Hu. 2020. Negative margin matters: Understanding margin in few-shot classification. In *European Conference on Computer Vision*. Springer, 438–455.
- [23] Lu Liu, Tianyi Zhou, Guodong Long, Jing Jiang, Lina Yao, and Chengqi Zhang. 2019. Prototype propagation networks (PPN) for weakly-supervised few-shot learning on category graph. *arXiv preprint arXiv:1905.04042* (2019).
- [24] Lu Liu, Tianyi Zhou, Guodong Long, Jing Jiang, and Chengqi Zhang. 2019. Learning to propagate for graph meta-learning. In *Advances in Neural Information Processing Systems*. 1037–1048.
- [25] Mingsheng Long, Yue Cao, Jianmin Wang, and Michael I Jordan. 2015. Learning transferable features with deep adaptation networks. *arXiv preprint arXiv:1502.02791* (2015).
- [26] Puneet Mangla, Mayank Singh, Abhishek Sinha, Nupur Kumari, Vineeth N Balasubramanian, and Balaji Krishnamurthy. 2019. Charting the Right Manifold: Manifold Mixup for Few-shot Learning. *arXiv preprint arXiv:1907.12087* (2019).
- [27] Nikhil Mishra, Mostafa Rohaninejad, Xi Chen, and Pieter Abbeel. 2017. A simple neural attentive meta-learner. *arXiv preprint arXiv:1707.03141* (2017).
- [28] Tsendsuren Munkhdalai and Hong Yu. 2017. Meta networks. In *ICML*. JMLR. org, 2554–2563.
- [29] Boris Oreshkin, Pau Rodríguez López, Alexandre Lacoste, et al. 2018. Tadam: Task dependent adaptive metric for improved few-shot learning. In *NeurIPS*. 721–731.
- [30] Tatdow Pansombut, Siripen Wikaisuksakul, Kittiya Khongkraphan, and Aniruth Phon-on. 2019. Convolutional Neural Networks for Recognition of Lymphoblast Cell Images. *Computational Intelligence and Neuroscience* 2019 (2019).
- [31] Siyuan Qiao, Chenxi Liu, Wei Shen, and Alan L Yuille. 2017. Few-shot image recognition by predicting parameters from activations. *CoRR*, abs/1706.03466 1 (2017).
- [32] Maithra Raghu, Chiyuan Zhang, Jon Kleinberg, and Samy Bengio. 2019. Transfusion: Understanding transfer learning for medical imaging. *arXiv preprint arXiv:1902.07208* (2019).
- [33] Sivaramakrishnan Rajaraman, Sameer K Antani, Mahdieh Poostchi, Kamolrat Silamut, Md A Hossain, Richard J Maude, Stefan Jaeger, and George R Thoma. 2018. Pre-trained convolutional neural networks as feature extractors toward improved malaria parasite detection in thin blood smear images. *PeerJ* 6 (2018), e4568.
- [34] Sachin Ravi and Hugo Larochelle. 2016. Optimization as a model for few-shot learning. (2016).
- [35] Andrei A Rusu, Dushyant Rao, Jakub Sygnowski, Oriol Vinyals, Razvan Pascanu, Simon Osindero, and Raia Hadsell. 2019. Meta-learning with latent embedding optimization. *ICLR* (2019).
- [36] Jake Snell, Kevin Swersky, Richard Zemel, et al. 2017. Prototypical networks for few-shot learning. In *NeurIPS*. 4077–4087.
- [37] Pavel Tokmakov, Yu-Xiong Wang, and Martial Hebert. 2019. Learning compositional representations for few-shot recognition. In *ICCV*. 6372–6381.
- [38] Eleni Triantafillou, Richard Zemel, and Raquel Urtasun. 2017. Few-shot learning through an information retrieval lens. In *NeurIPS*. 2255–2265.
- [39] Eleni Triantafillou, Tyler Zhu, Vincent Dumoulin, Pascal Lamblin, Utku Evci, Kelvin Xu, Ross Goroshin, Charles Gelada, Kevin Swersky, Pierre-Antoine Manzagol, et al. 2019. Meta-dataset: A dataset of datasets for learning to learn from few examples. *arXiv preprint arXiv:1903.03096* (2019).
- [40] Hung-Yu Tseng, Hsin-Ying Lee, Jia-Bin Huang, and Ming-Hsuan Yang. 2020. Cross-Domain Few-Shot Classification via Learned Feature-Wise Transformation. *arXiv preprint arXiv:2001.08735* (2020).
- [41] Oriol Vinyals, Charles Blundell, Tim Lillicrap, Daan Wierstra, et al. 2016. Matching networks for one shot learning. In *NeurIPS*.
- [42] Catherine Wah, Steve Branson, Peter Welinder, Pietro Perona, and Serge Belongie. 2011. The caltech-ucsd birds-200-2011 dataset. (2011).
- [43] Yu-Xiong Wang, Ross Girshick, Martial Hebert, and Bharath Hariharan. 2018. Low-shot learning from imaginary data. In *CVPR*. 7278–7286.
- [44] Flood Sung Yongxin Yang, Li Zhang, Tao Xiang, Philip HS Torr, and Timothy M Hospedales. 2018. Learning to compare: Relation network for few-shot learning. (2018).
- [45] Han-Jia Ye, Hexiang Hu, De-Chuan Zhan, and Fei Sha. 2018. Learning embedding adaptation for few-shot learning. *arXiv preprint arXiv:1812.03664* (2018).
- [46] Jason Yosinski, Jeff Clune, Yoshua Bengio, and Hod Lipson. 2014. How transferable are features in deep neural networks?. In *Advances in neural information processing systems*. 3320–3328.
- [47] Chi Zhang, Yujun Cai, Guosheng Lin, and Chunhua Shen. 2020. DeepEMD: Few-Shot Image Classification with Differentiable Earth Mover’s Distance and Structured Classifiers. In *Proceedings of the IEEE/CVF Conference on Computer Vision and Pattern Recognition*. 12203–12213.
- [48] An Zhao, Mingyu Ding, Zhiwu Lu, Tao Xiang, Yulei Niu, Jiechao Guan, Ji-Rong Wen, and Ping Luo. 2020. Domain-Adaptive Few-Shot Learning. *arXiv preprint arXiv:2003.08626* (2020).
- [49] Bolei Zhou, Aditya Khosla, Agata Lapedriza, Aude Oliva, and Antonio Torralba. 2016. Learning deep features for discriminative localization. In *CVPR*. 2921–2929.
- [50] Fengwei Zhou, Bin Wu, and Zhenguo Li. 2018. Deep Meta-Learning: Learning to Learn in the Concept Space. *arXiv preprint arXiv:1802.03596* (2018).
- [51] Linchao Zhu and Yi Yang. 2018. Compound memory networks for few-shot video classification. In *ECCV*. 751–766.